Study on the control of high ore pass dust pollution by pre-injection foam dedusting technology in the ore bin

Fabin Zeng (zengfabin0230@foxmail.com)
University of Science and Technology Beijing
Zhongan Jiang
University of Science and Technology Beijing
Yapeng Wang
University of Science and Technology Beijing

Research Article

Keywords: High ore pass, dust pollution, foaming agent, Gas-liquid ratio of foaming, foam dust reduction

Posted Date: June 9th, 2022

DOI: https://doi.org/10.21203/rs.3.rs-1661842/v1

Abstract

The impact airflow generated by ore unloading in the chute raises the dust carried by the ore itself and the floating dust and then the dust raised enters the roadway with the airflow and pollutes the environment. In order to minimize the amount of dust entering the roadway and reduce the pollution of unloading dust, we conducted an experimental study of selection of best foam formula and Pre-injection foam dust dedusting technology in ore bin. It was found that the optimal foaming formula was 1.0% SDBS + 0.5% SDS+(0.2%~0.4%)CMEA by the compound experiment using two evaluation criteria of initial foaming amount and foam defoaming rate. When the air pressure is 0.7MPa, the foaming rate of the foam generator is proportional to the gas and liquid flow rate and the best foaming gas and liquid flow ratio is 27.8. Under this circumstance, the foaming rate of the foaming formula is 500 L/min. When the height of foam is controlled at 15 cm, the effect of foam dust removal is the best. The dust emission rate from the foam to the fourth level can reach 60% and the dust fall rate of the third level is 28%, which effectively reduces the dust production and relieves the pressure of the spray hole dust fall at the wellhead.

1 Introduction

Multi-level high ore pass is common in mental mines, which provides great convenience for ore transportation. The raw rock extracted from the mine is crushed for the first time and then put into the ore pass transportation system through the mouth of the ore pass(Chen et al. 2017). Because the transport of ore passes into the ore bunker by gravity, the airflow in the pass is compressed rapidly during the free fall of a large amount of ore, this process breaks the stability of the airflow. Under the action of shear airflow, the fine dust in the ore and floating dust in the structure of the ore pass are raised quickly, and a large amount of dust enters the middle section of the lower part of the unloading port along with the airflow(Wang et al. 2017c), leading to the problem of dust pollution in the mine(Chen et al. 2016, Wang et al. 2020b). At the same time, with the increase of mining depth, the ore unloading gap gradually increases, dust pollution problem is also gradually intensified(Wang et al. 2020c). Therefore, it is very important to put forward an efficient dust removal measure to suppress dust pollution in the ore pass unloading process.

Up to now, many of dust pollution control of the multi-middle section high ore pass mine researches have focused on wellhead sealing and spray dust reduction of pass connecting roadway. In 1995, Xiang Liangdu (Xiang 1995) analyzed the calculation formula of impact air volume studied by professor Wang Yingmin of Northeastern University, proposed measures to control impact airflow from the aspects of unloading amount, unloading height and unloading section, so as to prevent dust from entering the roadway to pollute the working environment. In 2000, according to the theory of pressure relief dust control and the theory of dust removal and purification, Wang (Wang et al. 2000) put forward that a parallel dustproof pressure relief well should be dug near the main ore pass to connect the dustproof pressure relief well with the main ore pass to form a dustproof pressure relief ore pass system to control the dust pollution in the ore pass. In 2008, aiming at the dust production characteristics of the ore-unloading working space in metal mines, Wu (Wu 2008) designed a timing spray dust suppression

system for the ore-unloading working space. In 2013, Yang and LV (Yang &LV 2013) proposed a comprehensive dustproof measure for ore pass, that is, a fine water spray system was installed at the joint between the ore unloading chamber and the branch ore pass to reduce dust, and at the same time, a closed chain dustproof baffle was installed at each branch ore pass to seal and block the dust. In 2017, Wang Ming (Wang 2017) used numerical simulation to analyze the law of wind pressure at the unloading mouth and dust concentration in the ore pass. According to the law of dust migration, he proposed a gas-water spray dust removal scheme. In 2017, Li Yajun (Li et al. 2017) aimed at the problem that the dust production purification effect and purification capacity of high ore pass could not coexist, after studying the influence of liquid droplet inertia on dust deposition, they designed the atomization and dust removal device of high ore pass with large air volume. In 2019, Wang Yapeng analyzed the shielding effect of a high-pressure air curtain on the mine dust carried by the impact airflow of unloading on basis of CFD-DEM, determined the time when the air curtain blocked the continuous diffusion of dust and proposed a joint dust suppression scheme using high-pressure air curtain shielding and gas water spray.

On the whole, dust pollution control of the multi-middle section high ore pass is divided into external treatment and internal treatment. Although the above-mentioned dust suppression schemes which belong the former, such as air curtain and spray, can control dust pollution to a certain extent, there are some limitations in the field application. On the one hand, the nozzles of gas water spray are often blocked because of the impurities in the water supply network (Wei et al. 2020); On the other hand, the back and forth movement of the transport vehicles tends to make the air supply ducts leak (Li et al. 2022). These factors often lead to ineffective solutions for external dust removal and still large amounts of mine dust entering the working environment. This problem can be well solved by adopting foam dust removal technology inside the high ore pass. Foam dust removal refers to mixing foaming agent and aqueous solution according to a certain proportion to form foaming agent solution (Jiang 1990), introducing the foaming agent solution and air into the foaming device to foam, and injecting foam into the dust source by the foam nozzles to realize the suppression and sedimentation of dust (Weaire &Hutzler 1999). The pre-injected foam in the bin at the bottom of the high ore pass enables humidity, interception and adhesion of the dust carried by the impact airflow, which reduces the amount of dust produced from the source.

As for foam dust suppression technology, the research mainly focuses on the stability of the foam. Wang Hetang (Wang et al. 2017a, Wang et al. 2017b) analyzed the effects of foaming agent concentration and temperature on foam stability. Xu Chaohang (Xu et al. 2019, Xu et al. 2017) investigated the effect of anionic surfactants on the wetting properties of mineral dust and analyzed the effect of the foam stabilizer CMC on the stability of surfactant AES. WangQingguo (Wang et al. 2017d) investigated the properties of HPAM on SDBS foam solutions on the basis of the FoamScan. However, the foam formation mechanism and dust reduction mechanism are still unclear, and the measurement index of foam dust removal formulation is also unclear, which tends to cause blindness in foam preparation (Wang et al. 2019b). Simultaneously, foam dust removal technology in underground engineering fields, such as mines and tunnels, often needs to spray large amounts of foam (Wang et al. 2019a, Yan et al.

2020), which easily leads to unnecessarily high costs and seriously hinders the development of foam dust suppression technology.

The goal of this paper is to put forward the control of high ore pass dust pollution by pre-injection foam dedusting technology in the ore bin. We theoretically analyzed the formation mechanism of foam and the dust reduction model of foam, and determined the performance measurement index of foam dust removal formulation. We built up a similar experimental platform for dust reduction in high ore pass and used the experiment to determine the optimal dust removal foam formulation and foam dust removal parameters. The research results can relieve the pressure of spray dust removal outside the chute and improve the air quality of the mine working environment.

2 Dust Catching Mechanism Of Foam In Ore Bin

2.1 Mathematical model of foam formation mechanism

2.1.1 Mechanism of foam formation

Foam is a kind of gas-liquid dispersion medium, in which gas is the dispersed phase (discontinuous phase) and liquid is the dispersion medium (continuous phase). The foam is formed by the accumulation of bubbles on many sides. As shown in Fig. 1, the intersection of each bubble in the foam is defined as the *Plateau* boundary (Wei et al. 2020). Suppose the radius of the bubble is R, the pressure inside the bubble is p_A, the pressure outside the bubble is p_P, and the surface tension of the vacuolar membrane is σ. As the volume of bubbles increases dV, the surface area increases dA. Without considering other external forces, according to the first law of thermodynamics, there are (Jiang 1990):

$$\left(p_P - p_A\right)\mathrm{d}V + \sigma \mathrm{d}A = 0$$

1

If the shape of the foam is spherical, there are:

$$\frac{\mathrm{d}A}{\sim \mathrm{d}V} = \frac{8\pi R \mathrm{d}R}{4\pi R^2 \mathrm{d}R} = \frac{2}{R}$$

2

According to **formula (1)** and **formula (2)**, there are:

$$\Delta p = p_A - p_P = \frac{2\sigma}{R}$$

It is well known that bubbles are convex, and there will be $\Delta p > 0$. It can be seen from **formula (3)** that the pressure at point *P* in the liquid film is less than point *A*, so the liquid film automatically flows from point *A* to point *P*, and the liquid film gradually becomes thinner, which is the process of foam drainage. When the liquid film becomes thinner to a certain extent, it will lead to the rupture of the film and the destruction of the foam. Pure liquid cannot form stable foam, and some surface-active agents (foam stabilizers) are often added to the foam formulation, which can reduce the surface tension σ of the liquid film to relieve the time of foam drainage and make the generated foam more durable.

2.1.2 Mathematical model of foam coalescence

Foams are different in size at the beginning. More importantly, at this time, the foam is in a state of high surface free energy and extremely unstable, and there will be coalescence between the foam and the foam. The process of coalescence of large foam into small foam will reduce the surface-free energy of foam, thus forming a more stable foam. For the convenience of research, two adjacent foams are taken as research objects, and a foam coalescence model is established, as shown in Fig. 2. And make the following assumptions about the model (Ren 2009, Ren 2013):

The two foam contact surfaces are parallel flat plates, and gravity is not considered.

The liquid forming the liquid film is axisymmetric when flowing;

Ignore the other movements of the liquid forming the liquid film, only consider the radial movement, and the interface flows completely;

The flow field distribution of the fluid in the membrane is flat;

The fluid is a Newtonian fluid, which is incompressible and its viscosity value is certain.

The liquid film thinning rate is independent of radius *r*, and the liquid film pressure change is independent of *z*.

Therefore, when the two foams coalesce, the differential equation when only radial momentum is considered is:

$$\rho\left(\frac{\partial u_r}{\partial t}+u_r\frac{\partial u_r}{\partial r}+\frac{u_\theta}{r}\frac{\partial u_r}{\partial r}-\frac{u_\theta^2}{r}+u_z\frac{\partial u_r}{\partial z}\right)=-\frac{\partial p}{\partial r}-\left(\frac{1}{r}\frac{\partial}{\partial r}\left(r\tau_{rr}\right)+\frac{1}{r}\frac{\partial \tau_{r\theta}}{\partial \theta}-\frac{\tau_{\theta\theta}}{r}+\frac{\partial \tau_{rz}}{\partial z}\right)$$

4

According to hypothesis and hypothesis , **formula (4)** can be simplified as follows:

$$\rho\left(\frac{\partial u_r}{\partial t}+u\frac{\partial u_r}{\partial r}\right)=-\frac{\partial p}{\partial r}+u\left[\frac{\partial}{\partial r}\left(\frac{1}{r}\frac{\partial}{\partial r}ru_r\right)+\frac{\partial \tau_{rz}}{\partial z}\right]$$

5

For the flow field distribution of a flat plate, the influence of viscous force can be neglected, so the **formula (5)** can be further simplified as:

$$\rho\left(\frac{\partial u_r}{\partial t}+u\frac{\partial u_r}{\partial r}\right)=-\frac{\partial p}{\partial r}$$

6

The **formula (6)** is integrated along with the film thickness (z-direction), so there is:

$$\rho\left(\frac{\partial u_r}{\partial t}+\frac{1}{2}\frac{\partial \bar{u}_r^2}{\partial r}\right)=-\frac{\partial p}{\partial r}$$

7

Where,

$$\bar{u}_r^2=\frac{1}{h}\int_{-h/2}^{h/2}u_r^2\sim \mathrm{d}z=u_r^2$$

8

Because the liquid film is a parallel plate, the continuity equation of the two foam coalescence processes is:

$$-\pi r^2\frac{\mathrm{d}h}{\sim \mathrm{d}t}=2\pi rhu_r$$

9

Substituting **formula (9)** into **formula (6)**, there is:

$$\frac{\partial}{\partial t}\left(-\frac{r}{2h}\frac{\mathrm{d}h}{\mathrm{d}t}\right)+\left(-\frac{r}{2h}\frac{\mathrm{d}h}{\mathrm{d}t}\right)\frac{\partial}{\partial r}\left(-\frac{r}{2h}\frac{\mathrm{d}h}{\mathrm{d}t}\right)=-\frac{1}{\rho}\frac{\partial p}{\partial r}$$

10

Simplify **formula (10)** and integrate it along the radial direction, and there is:

$$\frac{\mathrm{d}^2h}{\mathrm{d}t^2}=\frac{3}{2h}\left(\frac{\mathrm{d}h}{\mathrm{d}t}\right)^2-\frac{4h}{\rho R^2}\Delta p \qquad (11)$$

Therefore, by combining **formula (3)**, the kinetic equation of spherical foam coalescence can be obtained as follows:

$$\frac{\mathrm{d}^2h}{\sim\mathrm{d}t^2}=\frac{3}{2h}\left(\frac{\mathrm{d}h}{\mathrm{d}t}\right)^2-\frac{4h}{\rho R^2}\frac{2\sigma}{R}$$

12

As can be seen from **formula (12)**, At the initial stage, the gas is dispersed in the liquid to form foams of different sizes. Since the newly formative foam is in a state of high surface free energy, the whole system is still in an unbalanced stage, at which time the foam will coalesce spontaneously. Big foams merge small foams, *i.e.*, merging between unstable foams. In this way, the foam system reduces the surface free energy as much as possible to reach a relatively balanced state system and form a relatively stable foam.

2.2 Mathematical model of foam dust suppression mechanism

In the process of dust production during ore unloading from the multi-middle section high ore pass, part of the dust directly enters the contact lane from the pass shaft, and the other part enters the ore bin with the ore. Pre-injection foam dedusting technology in the ore bin refers to pre-injecting foam generated by a foam generator into the ore bin before ore unloading in high ore pass, so as to wet, cover and block the floating dust. Compared with spray dust suppression, the foam has favorable isolation, adhesion and wettability (Chen et al. 2015, Lu et al. 2017), and has stronger wetting and covering effect on mine dust (Chen 2018). The theory of foam dust removal was analyzed from three aspects of foam wetting, interception and covering, adhesion, by which the performance parameters of the optimal foam formula are determined.

2.2.1 The mechanism of foam wetting

The process of dust wetting can be considered as the conversion of dust particles in contact with air to particles in contact with air and liquid at the same time (Chen et al. 2008). As shown in Fig. 3, the wetting of the dust by the foam is mainly manifested by the liquid film of the foam covering the surface of the dust particles evenly, when the foam is in contact with the surface of the dust particles. According to the Young equation, the wetting of the foam (Yang 2012) can be expressed by the contact angle θ in **formula (13)**.

$$\begin{cases} \sigma_{pg} - \sigma_{pl} = \sigma_{\mathrm{lg}} \cos\theta & \theta \in (0, \pi/2] \\ \sigma_{pl} - \sigma_{pg} = \sigma_{\mathrm{lg}} \cos\theta & \theta \in (\pi/2, \pi] \end{cases}$$

13

Whether the process can proceed spontaneously depends mainly on the difference value of free energy when the contact between mineral dust and the air is converted into the contact between mineral dust and liquid (Churaev 1995):

$$-\Delta E = -\sigma_{pl} + \sigma_{pg} + \sigma_{\mathrm{lg}} = W_a$$

14

Where, σ_{pl}represents free energy of solid and liquid interface per unit area, σ_{pg}represents free energy of solid and gas interface per unit area, σ_{lg} represents free energy of solid and liquid interface per unit area. The adhesive work W_{a} is defined as the work done to pull apart the liquid-solid interface per unit cross-sectional area. The larger the value of W_{a}, the stronger the adhesive properties of the liquid.

Substituting **formula (13)** into **formula (14)**, and there is:

$$W_a = (-\sigma_{pl} + \sigma_{pg})|1 + \sec\theta| \quad \theta \in (0, \pi]$$

15

For the dust produced by ore unloading in a high ore pass, the free energy of the solid and gas interface $\sigma_{pg}$of the dust particles is a fixed value. As can be seen from **formula (15)**, there is a negative correlation between adhesive work W_{a} and σ_{pl}. The main reason for hydrophobic mineral dust is that the surface tension σ_{pl} of mineral dust particles is too large when they contact with water. The foaming agent in the foam solution contains both hydrophilic and hydrophobic groups, which can make the mineral dust form a hydration film when it comes into contact with the solution. The hydrated film can effectively reduce the surface tension $\sigma_{pl}$and contact angle θ, and quickly change the hydrophobicity of mineral dust. The macroscopic performance is that the dust is wet and finally settles down. Therefore, foaming materials with high wettability can reduce the contact angle with mineral dust particles and improve the dust-catching effect of foam.

2.2.2 The mechanism of foam interception and covering

Dust particles move through the air. When the wind flow carrying dust passes through the foam, the obstructing wind flow effect of the foam causes a winding motion of dust particles within the local area of the foam. As shown in Fig. 4, When dust particles flow through the foam, and the minimum distance between the particle trajectory and the foam surface is equal to the particle radius r_p, the dust has the possibility of being caught by the foam, that is, the interception of the foam (Huang et al. 2008). When

the dust moves in a straight line with the airflow, it may be intercepted by the foam if the dust trajectory is within the critical trajectory.

Assuming that the foam is an ideal sphere with a diameter of d_f=2a and that the airflow around the sphere is a potential flow, then the flow function expressed in spherical coordinates is (Huang et al. 2008):

$$\phi = \frac{1}{2}\nu_0 \sin^2\alpha \left(R^2 - \frac{a^3}{R}\right)$$

16

The velocity component can be obtained as follows:

$$\begin{cases} u_R = \dfrac{1}{R^2 \sin\alpha}\dfrac{\partial \phi}{\partial \alpha} = v_0 \cos\alpha \left(1 - \dfrac{a^3}{R^3}\right) \\ u_\alpha = \dfrac{1}{R\sin\alpha}\dfrac{\partial \phi}{\partial \alpha} = -\dfrac{1}{2}\nu_0 \sin\alpha \left(2 + \dfrac{a^3}{R^3}\right) \end{cases}$$

17

On the surface of the ball, there are $u_R = 0$ and $u_\alpha = -\frac{3}{2}\nu_0 \sin\alpha$, Under the condition of potential flow, the interception efficiency around the sphere is:

$$\eta_\delta = \left(1 + \frac{d_p}{D_f}\right)^2 - \frac{D_f}{D_f + d_p}$$

18

If the interception parameter is set to, the interception efficiency can be converted to:

$$\eta_\delta = (1 + \delta)^2 - \frac{1}{1 + \delta}$$

19

Due to $\eta_\delta \in [0, 1]$, d_p satisfies:

$$0 \leqslant d_p \leqslant 0.324 D_f \quad (20)$$

The diameter of dust particles in the pass is much smaller than the diameter of foam, so it satisfies the **formula (20)**. On the macro level, the interception effect is manifested as the coverage performance of foam dust removal. When *n* foams separated by *h*□*a* act on the dust source at the same time, it is possible to intercept the dust within the foam 4*nh* range, as shown in Fig. 5. When the floating dust in the ore chamber of the ore pass is covered by a large amount of foam, the dust is mostly trapped.

2.2.3 The mechanism of foam adhesion

When the foam and dust move relative to each other at a certain speed, the dust is captured by the foam after the collision. Due to the gradual increase in mass after the accumulation of foam and dust, the liquid film on the upper surface of the foam gradually thins until it bursts due to gravity, and many small pieces of foam coated with dust fall to the ground (Wang et al. 2019c), as shown in Fig. 6.

The effect of adhesion can be expressed by adhesive force:

$$F_a = kd_p$$

21

Considering that the adhesive force of foam is influenced by the physical and chemical properties, viscosity, humidity, PH value and the nature of dust itself of each component in the foaming agent solution, it can be expressed by experience as:

$$F_a = kd_p(0.5 + 0.45RH)$$

22

Where, F_a represents the adhesive force, represents the adhesion coefficient of foam surface, d_p represents particle diameter, μm. RH represents the relative humidity of foam, %.

The foam dust removal process is usually not the result of a single effect, each effect plays a role, but the whole process is generally dominated by two or more effects. Foams can be seen as composed of single foam n_o, so total dust removal efficiency η is the sum of a single dust removal efficiency. When the dust removal efficiency of single foam remains unchanged, the total dust removal efficiency of foam increases with the number of foams. It is the premise of a good dust removal effect to produce a large amount of foam that is durable and has the function of wetting and collecting dust. Therefore, the best foaming formula can be measured and optimized from the two characteristics of foaming property and the stability of the foam.

3 Materials And Methods

3.1 Establishment of experimental platform for dust removal of ore pass

Based on the similarity criterion of the model of the main pass in an iron ore mine in Anhui province, the model of the similar pass is established on basis of the ratio of the size of the similar model to the actual size of 1:25 (Wang et al. 2020a). The size of the established similar model: the height of the slide is 3.6m, the height of each stratification is 0.80m, the diameter of the slide is 0.14m, the diameter of the bunker is 0.20m, the diameter of the slant slide is 0.12m (the Angle between the slant slide and the slide is 35°), the length of the contact roadway is 0.60m, the width of the contact roadway is 0.16m and the height of the contact roadway 0.18m. The testing equipment of the unloading experiment platform includes a microcomputer laser dust monitor (LD-5C) and multi-parameter wind speed monitor (JFY-4), which can realize real-time monitoring and recording of dust concentration and airflow changes at the wellhead during the unloading process, the established experimental platform for ore discharge through the pass is shown in Fig. 7. The dust concentration variation monitoring points are located at the mouths of each midsection ore pass. After the experimental ore discharge meets the similarity criteria, the single ore discharge is 1.28kg and the discharge flow is 0.64kg/s.

3.2 The experimental device and material for foam generation

Waring Blender method was used to determine the foaming formula. The experimental instruments used in the stirring method included: digital constant temperature water bath (HH-2), touch screen wet coagulation test agitator (MY3000), electronic balance, measuring cylinder and beaker, *etc*. As an auxiliary device for dust removal experiments, foam equipment provides foam for ore bunker (Jiang et al. 2014, Ren et al. 2009). The foaming device mainly includes air compressor (DakitaW-1.2/8), gas-water bag and foam generator(Internal mesh size: 2*2mm ~ 70 mesh). The foaming experimental device also includes value(KA-15), check value(AC-2000-M), pressure gauge(YTF-150), air flowmeter(LZT M-25), liquid flowmeter(LZT G-15), as shown in Fig. 8.

The necessary preparation materials of foam can be divided into two categories according to their properties: foaming agent and stabilizing agent. Considering that the agents would not affect the subsequent smelting process of metal mines on the basis of the existing research (Ni et al. 2019, Xie et al. 2020), five foaming agents (Sodium Dodecyl Sulfate(SDS), Sodium Dodecyl Benzene Sulfonate(SDBS), Sodium Alpha-olefin Sulfonate(AOS), Dodecyl Dimethyl Betaine(BS-12), Sodium Oxyethylene Ether Sodium Sulfate (AES)) and three foam stabilizers (Anionic Polyacrylamide (PAM), Sodium Carboxymethyl Cellulose CMC-Na and Coconut Oil Monoethanolamide (CMEA)) were selected.

4 Results And Discussion

4.1 Foam formulation performance test

4.1.1 Single foaming agent foaming experiments and optimization

Single-agent foaming experiments were conducted for the above five foaming agents on basis of Waring Blender method (Chen et al. 2015). Firstly, according to the characteristics of each foaming agent, 100ml of foaming agent solutions with different mass concentrations are prepared. Secondly, stir at the speed of 1000r/min for 1min, immediately pour the foam into the measuring cylinder after stopping the rotation, and obtain the foam volume initial to characterize the foaming property of the foaming agent. Then the foam volume after 5 minutes was recorded to characterize the stability of the foaming agent. Three sets of experiments were repeated for each blowing agent and an average of the foam volumes was calculated.

The results of the single-agent foaming experiment are shown in Fig. 9. It could be seen from the standard deviation in Fig. 9 that the dispersion degree of experimental data was small, and the standard deviation of foam volume of initial and foam volume after 5 minutes was basically within 10%, so the obtained data were considered to be stable and reliable.

It can be seen from Fig. 9 that with the increase of the mass concentration of the solution, the initial foam volume of a single blowing agent firstly increases and then decreases slowly, and the variation law of the average defoaming rate of different blowing agents is also different. From the theoretical analysis of adsorption (Wang et al. 2019c), it can be seen that when the concentration of foaming agents is low, the surface adsorption is sparse. With the increase of the mass concentration of the foaming agent, the surface adsorption becomes denser and denser, the surface tension decreases, and the foaming volume increases rapidly. When the concentration increased to the critical concentration of the beam glue (Williams et al. 1955), the surface adsorption reached saturation, and the increase of the concentration did not increase the surface adsorption amount. According to the initial foaming volume and the average rate of foam disappearance, the foaming agents with favorable foaming performance were SDS, SDBS and AES, and the optimal mass concentration was 0.5%, 0.3% and 0.5%, respectively.

4.1.2 Experiment of compounding foaming agent monomer

Pairwise compounding experiments of the three preferred blowing agents were performed to determine the effect of a component on the foaming properties. The mass concentration of the compounding agent was respectively set to be 0–2.0 times that of the agent to be compounded, and the interval of the times was set to be 0.5 in the experiment. The Waring Blender stirring method was used to repeat the experiments in three groups and calculate the average volume of the foam. The results of the foaming agent compounding experiment are shown in Fig. 10.

It can be seen from Fig. 10 that:

1)With the increase of $c_{(SDS)}/c_{(SDBS)}$, the initial foam volume shows a trend of sharp increase and then slowly decrease. This was because both SDS and SDBS were anionic forming agents (Wang et al. 2017d). When the concentration of their combination was lower, the active groups interacted to reduce the surface tension and increase the foaming volume. However, as the concentration increases, the synergistic effect reaches equilibrium (Wei et al. 2020), the surface tension no longer decreases and the foaming volume reaches a maximum. As the concentration increases further, the foam volume decreases due to the inhibitory effect of too many free radicals on the foam.

2)With the increase of $c_{(AES)}/c_{(SDBS)}$, the initial foam volume shows a trend of rapid increase at first and then tends to be stable. The adsorption layer produced by AES was repelled by the same charge, so the molecules were not arranged closely enough and the cross-sectional area of the molecules was large. After the addition of SDBS, due to the hydrophobic effect and the generated dipole-ion interaction (Wang et al. 2019a), it is easy to be inserted into the loose adsorption layer, reducing the repulsion of the same charge, and increasing the density of the hydrophobic chain, so the molecules are arranged more closely, resulting in the reduction of the surface tension and the increase of the foaming volume. When the concentration went up to a definite value, the synergistic effect no longer produced effects and the foam volume also tended to be stable.

3)There was no significant relationship between the initial foam volume and the concentration ratio of $c_{(AES)}/c_{(SDS)}$.

When $c_{(SDS)}/c_{(SDBS)} = 0.5$, the initial foam volume of this group of compound experiments is much higher than that of other groups of compound experiments, and the foaming effect is also higher than that of a single foaming agent. To determine the optimal content of the composite foaming agent of SDS-SDBS, in view of the condition that $c_{(SDS)}/c_{(SDBS)} = 0.5$, the experiments were conducted with the mass concentration of the composite foaming agent set at 0.5 ~ 3%, and the concentration interval at 0.5%, respectively. The experimental results are shown in Fig. 11. It could be seen from the figure that the initial foam volume firstly increased sharply and then basically stabilized with the increase of the concentration of the compounded foaming agent. In order to ensure the optimal foaming effect and economy, the optimal mass concentration of the SDS-SDBS compound foaming agent was 1.5%, under which $c_{(SDS)}$ was 0.5% and $c_{(SDBS)}$ was 1%.

4.1.3 Experiment of compound foaming agent and foam stabilize

When the mass concentration of the SDS-SDBS combined blowing agent was 1.5%, the optimal initial foam volume was 622ml, but the average defoaming rate was as high as 19.72ml/min within 5min, and the stability was weaker than that of the single foaming agent. Therefore, in order to improve the stability of the compounded foaming agent, three foam stabilizers, namely, PAM, CMC-Na and CMEA, were added for the optimization experiment. Experiments were performed by setting the mass concentration of foam

stabilizer to be 0 ~ 1%, with the concentration interval of 0.2% and the average volume of foam disappearance during 5 minutes as shown in Fig. 12. The foam stabilizing effect of CMEA is better. With the increase of CMEA content, the foam stabilizing effect firstly increases and then decreases, and the optimal mass concentration range is 0.2 ~ 0.4%.

Therefore, the optimal foaming scheme was determined through the performance test of foaming agent formulation: $c_{(SDS)}$ = 0.5%, $c_{(SDBS)}$ = 1%, $c_{(CMEA)}$ = 0.2 ~ 0.4%.

4.2 Measurement experiment of mineral dust discharge in ore pass

The ore enters the transportation system from the slip well to form an ore flow, which falls freely by gravity and is accompanied by a large amount of dust. Through on-site monitoring and similar experimental analysis, it can be seen that the dust in the ore pass mainly gushed out from the third and fourth levels when the first middle level was unloaded. The unloading of mineral dust in the pass shaft is mainly reflected in two aspects: the dust carried by the ore is generated by the sheer airflow during the falling process, and the dust attached to the inner wall of the pass shaft is secondary dust generated by the impact of the ore and the airflow. The pre-injection of foam in the ore bin mainly controls the floating dust in the ore bin, so the ore unloading experiment is conducted to determine the dust yield of the floating dust.

In order to distinguish the percentages of different dust sources, the controlled variable method was used to conduct three groups of controlled experiments (α, β, γ) with different ore unloading conditions on the basis of unchanged ore unloading amount and ore unloading flow. The settings of the experimental groups were as follows: experiment α was used as the control group of the other two groups for normal ore unloading; experiment β laid flexible materials at the bottom of the ore bunker to absorb the falling impact energy of ore and prevent the dust from the recoil flow in the ore bunker; experiment γ is the influence of another ore unloading experiment on the dust deposit in the ore bunker after two consecutive ore unloading. The Settings of the three experiments and the monitoring of dust concentration are shown in Fig. 13.

The changes in dust concentration in the three groups of control experiments were measured by the dust concentration monitor. The dust concentration under different conditions was shown in Fig. 14. It can be seen from Fig. 14 that the amount of dust released from the shear gas during ore falling is greater than the amount of dust released from the re-collision when the ore falls into the ore bin. The amount of dust produced during ore unloading accounts for 78% of the total amount of dust produced, and the amount of dust produced after the ore falls into the ore bin accounts for 22%. When there is floating dust in the ore bin, the dust production in the ore pass increases obviously after ore unloading again, and the dust production in the ore bin increases by 39% compared with that when there is no floating dust. The use of foam to inhibit the floating dust at the bottom of the ore bin can play a role in reducing the overall production of dust.

4.3 Experimental analysis of foam dust removal

Through the control variable method for the unloading experiment, we can know that the dust output of floating dust at the bottom of the warehouse reaches 39%, so it is significant to adopt the pre-injection foam to control the dust in the warehouse. In order to improve the foaming effect and boost the dust removal rate, based on the above formula, the foaming experiment was carried out by using the foam-collecting system in the pass shaft. When the foaming equipment is unchanged, the change in gas-water flow has a great influence on the foaming quantity.

In order to study the relationship between foaming quantity and gas-water flow ratio, the control variable method is adopted to select the gas flow as 10, 15, 20, 25 and 30 m^3/h and the liquid flow as 4, 8, 12, 16 and 20L/min on the basis of setting the pressure empirical value as 0.7MPa for monitoring the foaming flow. The relationship between foaming flow and gas-water flow is shown in Fig. 15. When the gas flow reached 30 m^3/h, the foaming speed increased first and then stabilized with the increase of water flow. When the pressure is constant, the foaming rate decreases with the increase of the gas-water ratio. When the water pressure is constant, the foaming rate increases with the increase of the gas-water ratio. Through data analysis, it is found that when the gas flow is 30 m^3/h, the liquid flow is 18L/min, the optimal gas-water ratio is 27.8, and the foaming agent has the best foaming effect.

Based on the optimal foaming gas-water ratio of 27.8 obtained in the above study, the dust control effect was studied by injecting foam of different heights (the height of foam in the ore bunker is 0cm, 5cm, 10cm, 15cm and 20cm) into the ore pass. As the dust returning from the ore bin is mainly reflected in the third and fourth levels of the ore pass during ore unloading at the first middle level, only the dust changes at the third and fourth levels are monitored. The influence of foam of different heights on dust concentration change in the third and fourth middle sections after unloading is shown in Fig. 16.

Through the unloading experiment after filling different heights of foam in the ore chute bin, the analysis of experimental data shows that with the increase of the foam height in the ore pass bin, the concentration of dust flushed out from the ore chute mouth decreases gradually. From the histogram of dust control efficiency at the wellhead of the third and fourth levels in Fig. 16, it can be seen that the total dust reduction rate of foam in the ore bin for the fourth middle section is 60%, and that for the third middle section is 28%. Among them, the dust reduction effect of respirable dust is lower than that of total dust. The pre-injection of foam in the ore bin controls the dust return amount in the ore bin, weakens the total amount of dust entering the third and fourth levels of the ore pass, and relieves the pressure of spray dust reduction at the ore pass mouth to a greater extent.

5 Conclusions

1) From the perspectives of the mechanism of foam formation, the dynamic process of foam coalescence, and energy conversion during contact between foam and dust in the ore bin, it is concluded

that the pre-injected foam dust removal mainly includes three effects: foam wetting, interception and covering, and adhesion.

2) The best foaming formula was determined as: 0.5% sodium dodecyl sulfate SDS + 1.0% SDBS sodium dodecyl benzenesulfonate + (0.2% ~ 0.4%) CMEA coconut oil monoethanolamide according to the initial foaming volume and the foam volume after 5 minutes through the experiments of foaming with a single agent and the compounding of two agents.

3) Foaming equipment was used to conduct the foaming performance (foaming rate) experiment. When the pressure was 0.7 MPa, the foam flow increased with the increase of liquid flow and gas flow, and the foaming speed tended to be stable at last. When the gas flow is 30m^3/h, the water flow is 18L/min, and the foaming rate of the foaming agent is the fastest 500 mL/min, at which time the gas-water ratio is 27.8.

4) Under the condition that foam is pre-injected into the slip hole model and the foam injection height is changed, it was found that when the foam injection height was 15cm, the control effect of dust removal in the fourth middle section could reach 60%, and the dust removal rate in the third middle section was 28%. The pre-injection foam reduces the total amount of dust entering the flow connection lane, reduces the external dust removal workload, and achieves a better dust removal effect.

Declarations

Ethical Approval

Not applicable.

Consent to Participate

Not applicable.

Consent to Publish

Not applicable.

Authors Contributions

Fabin Zeng Writing - Original Draft, Conceptualization, Methodology

Professor Zhongan Jiang Supervision, Funding acquisition, Writing - Review & Editing

Yapeng Wang Writing - Original Draft, Investigation

Acknowledgement

This work was supported by Natural Science Foundation of China(51874016).

Conflict of Interest

The authors declare that they have no known competing financial interests or personal relationships that could have appeared to influence the work reported in this paper.

Availability of data and materials

The data used to support the findings of this study are available from the corresponding author upon request.

References

1. Chen J, Jiang Z, Jiang L, Wang M (2015) Formulation and experimental study of foam dust suppressant for downhole drill in open pit mine. J China Coal Soc 40:132–138
2. Chen J (2018) Property experiments on the foam generator and its influencing factors during down-the-hole drilling. Process Saf Environ 114:169–178
3. Chen JP, Hazra A, Levin Z (2008) Parameterizing ice nucleation rates using contact angle and activation energy derived from laboratory data. Atmos Chem Phys 8:7431–7449
4. Chen L, Wu C, Chen Z, Yao G, Xiao Z (2016) Simulation analysis of factors affecting the impact gas flow in the shaft. Min Res Dev 36:83–87
5. Chen Y, Wang M, Jiang Z, Cheng J, Sun Y (2017) Numerical simulation of the generation law of impulsive airflow in high ore pass and its influencing fac-tors. J China Coal Soc 42:178–185
6. Churaev NV (1995) Contact angles and surface forces. Adv Colloid Interface Sci 58:87–118
7. Huang B, Wang D, Shi G, Li D (2008) Theoretical study on the mechanism of foam dedusting. Industrial Safety and Environmental Protec-tion, pp 13–15
8. Jiang Z (1990) Wet dust removal technology and its application. China Coal Industry Publishing House, Beijing
9. Jiang Z, Jiang L, Chen J (2014) Formulation and experimental study of foam dust sup-pressant for downhole drill in open pit mine. J China Coal Soc 39:903–907
10. Li Y, Liu W, Li Y, Wang Z, Liu D (2017) Research and application of atomizing dust removal device with high air volume in high ore pass. Hunan nonferrous metals 33:7–8
11. Li Y, Wang Q, Tuo L, Zhang F, Zhang X (2022) : Experimental investigations of a novel pressure microfoam preparation device for dust removal. SCIENCE AND ENGINEERING OF COMPOSITE MATERIALS 29, 1–8
12. Lu X, Zhu H, Wang D (2017) Investigation on the new design of foaming device used for dust suppression in underground coal mines. Powder Technol 315:270–275
13. Ni GH, Qian S, Meng X, Hui W, Xu YH, Cheng WM, Gang W (2019) : Effect of NaCl-SDS compound solution on the wettability and functional groups of coal. Fuel 257

14. Ren W (2009) : Research on theory and technology of foam dust removal in coal mine. å□šå£« Thesis, China University of Mining and Technology
15. Ren W, Wang D, Wu B, Wang B, Liu W (2009) Mine foam dust control technology. Coal Sci Technol 37:30–32
16. Ren W (2013) Research on theory and Technology of foam dust removal in underground coal mine. China University of Mining and Technology press, Xuzhou
17. Wang F, Gou g, Wang Y, Wang B, Shi c, Wen Z, Tian K, Deng D Y (2000) Study on comprehensive technology of pressure relief dedusting and purification of pass. Nonferrous Metals(Mining), pp 43–45
18. Wang H, Chen X, Xie Y, Wei X, Liu WV (2019a) Experimental study on improving performance of dust-suppression foam by magnetization. Colloid Surf A 577:370–377
19. Wang H, Wei X, Du Y, Wang D (2019b) Experimental investigation on the dilatational interfacial rheology of dust-suppressing foam and its effect on foam performance. Process Saf Environ 123:351–357
20. Wang H, Wei X, Du Y, Wang D (2019c) Effect of water-soluble polymers on the performance of dust-suppression foams: Wettability, surface viscosity and stability. Colloid Surf A 568:92–98
21. Wang HT, Guo WB, Zheng CB, Wang DM, Zhan HH (2017a) Effect of Temperature on Foaming Ability and Foam Stability of Typical Surfactants Used for Foaming Agent. J Surfactants Deterg 20:615–622
22. Wang HT, Li J, Wang Z, Wang DM, Zhan HH (2017b) Experimental Investigation of the Mechanism of Foaming Agent Concentration Affecting Foam Stability. J Surfactants Deterg 20:1443–1451
23. Wang M (2017) : Study on mechanism and time-space distribution characteristics and control technology of high ore pass dust. Thesis, University of Science and Technology Beijing
24. Wang M, Jiang Z, Chen J, Deng q (2017c) Similarity theory and experimental study on influenc-ing factors of high ore pass mine unloading impinging airflow. Vib shock 36:276–282
25. Wang Q, Wang D, Shen Y, Wang H, Xu C (2017d) Influence of polymers on dust-related foam properties of sodium dodecyl benzene sulfonate with Foamscan. J Disper Sci Technol 38:1726–1731
26. Wang YP, Jiang ZG, Wang JZ, Zheng DF, Chen JH, Yang B, Wang M (2020a) : The visualization study of dust pollution generated during unloading of the multi-level in high ore pass based on CPFD software and similar experiments.J Clean Prod256
27. Wang YP, Jiang ZG, Wang JZ, Zheng DF, Wang M (2020b) Research on Control of Ore Pass Dust by Unloading Time Interval and Foam Control Technology. Acs Omega 5:16470–16481
28. Wang YP, Jiang ZG, Xu F, Wang JZ, Zhang GL, Zeng FB (2020c) Study on Parameters of a New Gas-Water Spray in Ore Pass Dedusting Based on Experiment and Numerical Simulation. Acs Omega 5:21988–21998
29. Weaire D, Hutzler S (1999) :The Physics of Foams

30. Wei X, Wang H, Xie Y, Du Y (2020) An experimental investigation on the effect of carboxymethyl cellulose on morphological characteristics of dust-suppression foam and its mechanism exploration. Process Saf Environ 135:126–134
31. Williams RJ, Phillips JN, Mysels KJ (1955) The critical micelle concentration of sodium lauryl sulphate at 25° C. Trans Faraday Soc 51:728–737
32. Wu G (2008) : Optimization of mine ventilation system and dust con-trol technology in typical nonferrous metal mines. å□šå£« Thesis, Central South University
33. Xiang L (1995) Technical measures to control the impact of ore slip-ping on wind current. Eng Constr 6:43–45
34. Xie HC, Ni GH, Xie JN, Cheng WM, Xun M, Xu YH, Wang H, Wang G (2020) The effect of SDS synergistic composite acidification on the chemical structure and wetting characteristics of coal. Powder Technol 367:253–265
35. Xu C, Wang D, Wang H, Zhang Y, Dou G, Wang Q (2017) Influence of gas flow rate and sodium carboxymethylcellulose on foam properties of fatty alcohol sodium polyoxyethylene ether sulfate solution. J Disper Sci Technol 38:961–966
36. Xu C, Wang D, Wang H, Ma L, Zhu X, Zhu Y, Zhang Y, Liu F (2019) Experimental investigation of coal dust wetting ability of anionic surfactants with different structures. Process Saf Environ 121:69–76
37. Yan JY, Nie W, Zhang HH, Xiu ZH, Bao Q, Wang HK, Jin H, Zhou WJ (2020) Synthesis and performance measurement of a modified polymer dust suppressant. Adv Powder Technol 31:792–803
38. Yang J (2012) Principle and application of surfactant. Southeast University Press, Nanjing
39. Yang K, LV S (2013) Study on the treatment of impact dust in the ore chute of Tongxing company. Nonferrous Metals(Mining) 65:68–70

Figures

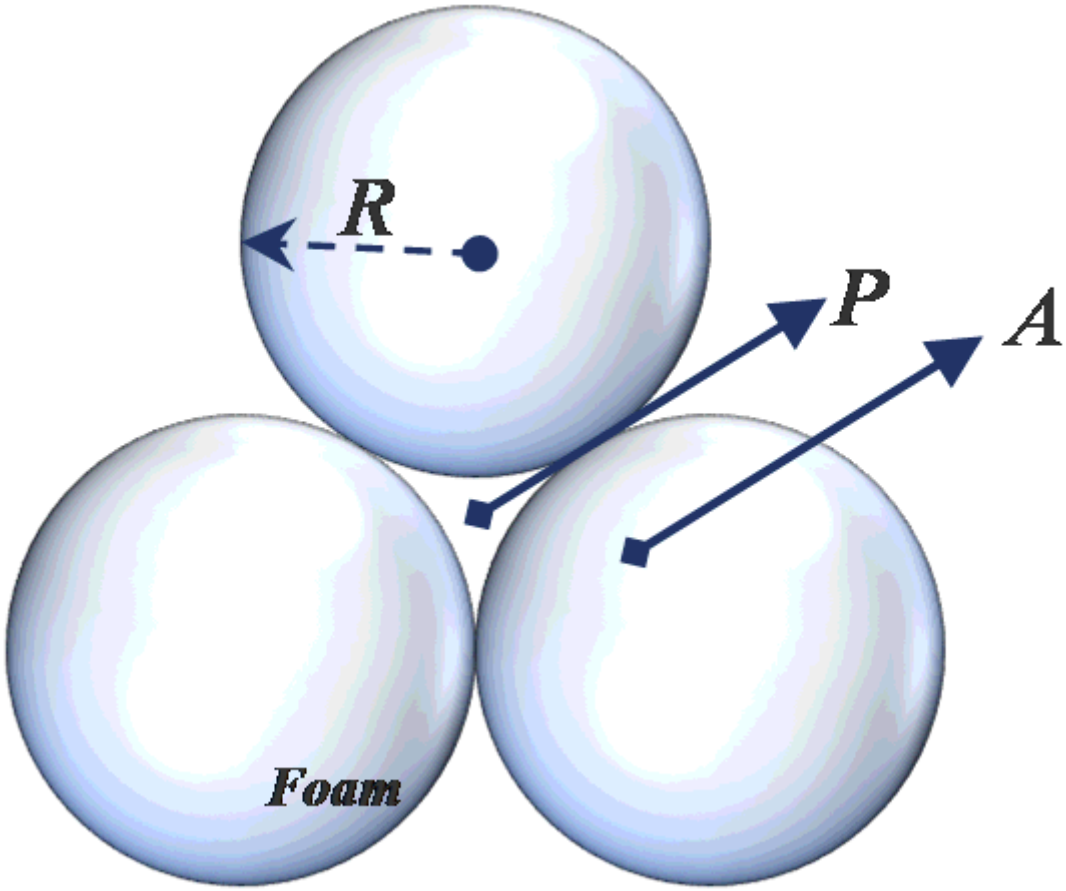

Figure 1

Schematic diagram of *Plateau* boundary

Figure 2

Schematic diagram of foam coalescence

Figure 3

Schematic diagram of contact angle during foam wetting

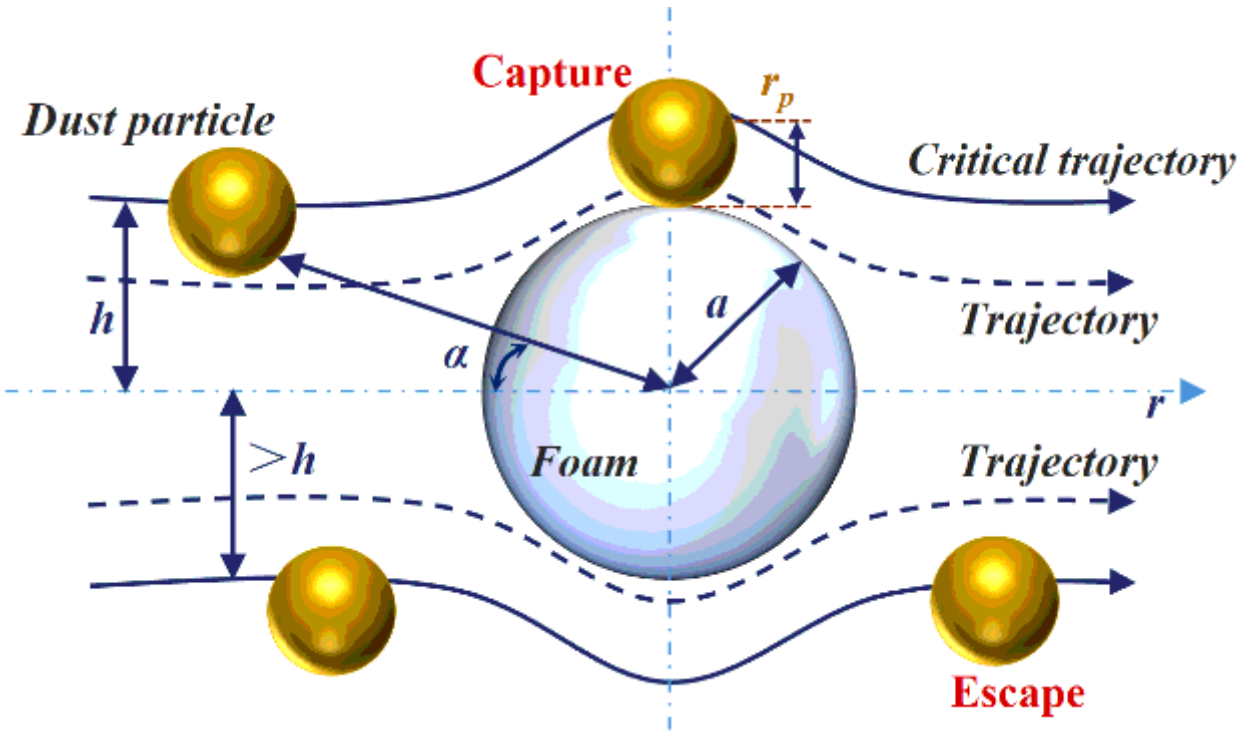

Figure 4

Schematic diagram of foam interception effect

Figure 5

Schematic diagram of foam blanket effect

Figure 6

Schematic diagram of foam adhesion effect

Figure 7

Experimental platform for ore unloading of multilevel high ore pass

Figure 8

Foaming experimental device diagram

Figure 9

The foaming volume of single substance

Figure 10

Experimental results of blowing agent compounding

Figure 11

Foaming of SDS and SDBS at different concentrations

Figure 12

Foam stabilizer to slow down defoaming

Figure 13

Experimental settings and analysis of dust production in the ore pass

Figure 14

Analysis of dust production in each stage of ore unloading in ore pass

Figure 15

relationship between gas flow rate and foaming flow rate

Figure 16

Foam fall rate in mine bin